

# Improving inference on neutron star properties using information from binary merger remnants

Tamanna Jain<sup>1,\*</sup> and Michalis Agathos<sup>2,1,†</sup>

<sup>1</sup>*Department of Applied Mathematics and Theoretical Physics,  
University of Cambridge, Wilberforce Road CB3 0WA Cambridge, United Kingdom.*

<sup>2</sup>*Queen Mary University of London, Mile End Road, London, E1 4NS, UK.*

(Dated: April 19, 2024)

The gravitational-wave signal GW170817 is a result of a binary neutron star coalescence event. The observations of electromagnetic counterparts suggest that the event didn't lead to the prompt formation of a black-hole. In this work, we first classify the GW170817 LIGO-Virgo data sample into prompt collapse to a black-hole using the  $q$ -dependent threshold mass fits and then remove these cases from the data sample. We find that the cases without a prompt black-hole formation do not support radii  $< 10$  km unlike the LIGO-Virgo data sample. This is consistent with the maximum mass constraint, based on the binary pulsar J0348+0432, imposed LIGO-Virgo data sample. Additionally, we find that the cases without the prompt collapse to a black-hole improve the uncertainty range of neutron star radii from 3.3 km to 2.6 km for the data sample without the mass constraint and from 2.8 km to 2.5 km for the data sample with the mass constraint, implying improved constraints on the neutron star radii and hence the equation-of-state.

## I. INTRODUCTION

In 2015, the first gravitational-wave (GW) detected from the merger of a binary black-hole (BBH) [1] by the LIGO-Virgo detectors [2, 3] opened a new era of GW astronomy. Subsequently, LIGO-Virgo detected GW signals from coalescence of binary neutron-star (BNS) systems, namely GW170817 [4–6] and GW190425 [7].

The merger of a BNS system can lead either to a prompt collapse to a BH or a formation of a NS remnant (non-prompt collapse) [8–14], that can be either stable or unstable, depending on its mass and spin. The detection of electromagnetic (EM) counterparts from space-based or ground-based observatories is crucial to identify the signal from the BNS merger as a non-prompt collapse signal. The EM radiation emitted can either be from the dynamical ejection of neutron-star matter, or from the formation of a disk surrounding the remnant. The follow-up searches after the detection of the GW signal led to the observation of EM counterparts in the case of GW170817, while in the case of GW190425 no EM signal was detected. The EM counterpart of GW170817, known as AT2017gfo, consisted of a short gamma ray burst (sGRB) [15–17] followed up by strong emission from X-ray to radio [18–23], that was compatible with a kilonova transient event, and pointed to a non-prompt collapse merger. There could be many reasons for the lack of detection of the EM counterparts for GW190425. Due to its poor sky-localization ( $8284 \text{ deg}^2$  as its 90% confidence region, compared to  $28 \text{ deg}^2$  for GW170817), and its large distance ( $159^{+69}_{-71} \text{ Mpc}$  compared to  $\sim 40 \text{ Mpc}$  for GW170817), it was very unlikely that a low-latency survey would have picked up such a faint source while

having to cover such a wide patch. It is also possible that the EM emission was highly collimated and that our line of sight lied outside the source's emission cone.

Over the years, various numerical relativity (NR) studies investigated the remnants of BNS mergers, concluding that the coalescence of a BNS system is followed by the prompt collapse to a BH if the total mass of the binary is greater than some characteristic mass called the threshold mass. Thus, accurate modelling of this threshold mass is important as it characterizes the outcome of the merger remnant for a BNS of a given total mass. The first use of the non-prompt-collapse hypothesis for GW170817 was made in Ref. [24] to place a bound on the NS radius,  $R_{1.6} > 10 \text{ km}$ , for a fiducial NS mass of  $1.6 M_{\odot}$ .

In recent works, Bauswein *et al.* [26] and Kölsch *et al.* [27] provide empirical formulae for the threshold mass, as a function of the equation of state (EOS) of NS matter and the mass ratio of the BNS, based on NR simulations. In this work we make use of these fits and the presence of an EM counterpart for GW170817 event to improve the inference on the properties of NS matter. On applying this method to GW170817 we find that a significant part of the parameter space is not supported by the observation of the EM counterpart.

The paper is organised as follows. In Sec. II, we briefly discuss NR simulation techniques used in Refs. [26–28] and the range of EOSs and mass-ratios  $q$  used in these studies. Section III first outlines the method based on which we classify the outcome of the BNS merger and then the Bayesian analysis used for GW170817. Finally, we present our results for the GW170817 signal, along with the results from the injection studies of Ref. [28] in Sec. IV with concluding remarks in Sec. V.

\* tj317@cam.ac.uk

† m.agathos@qmul.ac.uk

## II. OVERVIEW OF NUMERICAL SIMULATIONS OF NEUTRON STAR BINARIES

In this section, we discuss the numerical techniques and the set up of the BNS systems used in Bauswein *et al.* [26] and Kölsch *et al.* [27] to study the impact of mass-ratio on the onset of a prompt-collapse to a BH.

The different groups use independent NR codes on similar binaries for their analysis. The NR simulations of Kölsch *et al.* use BAM code for dynamical evolutions which is based on the 3+1 decomposition of Einstein’s Equation in the Z4c formalism [29, 30]. The (1 + log) slicing and gamma-driver gauge conditions are used for lapse and shift, respectively [31–33]. BAM uses nested Cartesian grids to solve both the general relativistic hydrodynamics (GRHD) equations and the Einstein’s equations. On the other hand, the smoothed particle hydrodynamics (SPH) code [34–36] used by Bauswein *et al.* employs the conformally flat approximation of general relativity to solve Einstein’s equations [37, 38]. The SPH code uses the Lagrangian particle method to solve the equations of GRHD [39] and the multigrid solver to solve the field equations. The particle mesh codes are then used to translate between the SPH particles and the gravity grid [40]. BAM utilises AMR (adaptive mesh refinement) techniques [41] whereas the multilevel adaptive technique [42] is used in SPH for solving nested grid setup.

For their analysis, Kölsch *et al.* consider 290 NR simulations with varying total mass, and mass-ratios  $q$ , ranging from  $0.57 \leq q \leq 1$ . They consider a restricted set of 3 EOSs, namely ALF2 [43], SLy [44], and H4 [45] such that their maximum mass is compatible with the observation of binary pulsar J0348+0432 [46]. The maximum mass of non-rotating NSs corresponding to these EOSs are  $1.99 M_{\odot}$ ,  $2.06 M_{\odot}$  and  $2.03 M_{\odot}$ , respectively. However, as mentioned in Kölsch *et al.* due to a small set of EOSs, the  $M_{\text{thr}}$  fit based only on their data does not reliably predict  $M_{\text{thr}}$  for other NR simulated EOSs given in Perego *et al.* [47]. Therefore, as in Kölsch *et al.* we would consider a fit derived from both the data [25, 27, 47] (Table X of [27]) for our analysis. On the other hand, Bauswein *et al.* consider a total of 40 EOS models, out of which 23 are hadronic EOS models which they refer to as their “base sample” [43, 44, 48–66], 8 belong to the “excluded hadronic sample” of EOSs [45, 58–61, 67–69] and the remaining 9 are EOSs which include a phase transition to deconfined quark matter called ‘hybrid’ EOS models [54, 70–75]. They consider three mass-ratios, namely 1.0, 0.85 and 0.7. Based on the classification of the EOS models, Bauswein *et al.* present the threshold mass fit formula for each EOS model as well as for the combinations of EOS models. As the EOSs considered in Kölsch *et al.* and Perego *et al.* are included in the base and excluded EOS models of Bauswein *et al.*, we only consider the threshold mass fit formula for the “base+excluded” model for our analysis on GW170817.

To verify the robustness of the two  $q$ -dependent threshold mass fits presented in Bauswein *et al.* and Kölsch *et al.*

*al.*, we use these fits on the 17 NR studies considered in Agathos *et al.* [28]. In that study, the authors used previously presented NR simulations data from Refs. [76–82] along with the two NR simulations performed on the WhiskyTHC code [83–85]. The study considers mass-ratios ranging from  $0.86 \leq q \leq 1.0$  with a total of 8 EOSs, out of which 5 are microphysical EOSs: BHBA $\phi$  [48], DD2 [51, 52], LS220 [58], SFHo [62], SLy-SOR [86] and the remaining 3 are piecewise polytropic EOSs: ALF2, 2B and SLy [66].

## III. METHODS

In this Section we detail the methods used to i.) establish numerical fits relating the progenitor binary parameters to the nature of the merger remnant and ii.) perform Bayesian inference on the GW data from a BNS signal in order to recover an improved measurement on NS matter properties, with a focus on GW170817.

### A. Numerical fits for remnant classification

The threshold mass ( $M_{\text{thr}}$ ) can be used to reliably classify the merger remnant in the NS binaries, that is, if the total mass  $M$  of the NS binary is larger than the threshold mass, then the merger product is a prompt collapse to a BH. It is convenient to express the threshold mass as

$$M_{\text{thr}} = k_{\text{thr}} M_{\text{max}}^{\text{TOV}}, \quad (3.1)$$

where,  $k_{\text{thr}}$  is a coefficient greater than unity that depends on the EOS, the mass-ratio  $q$  and the spins, and  $M_{\text{max}}^{\text{TOV}}$  is the mass of the heaviest stable non-rotating NS supported by the EOS. The validity of this expression was first established using large sets of NR hydrodynamical simulations [11, 12].

For a sample of 12 hadronic EOSs and equal-mass binaries, Ref. [12] observed an approximate EOS-independent linear relation between  $k_{\text{thr}}$  and the maximum compactness of the non-rotating NS ( $C_{\text{max}}$ ). For a fixed mass-ratio of  $q = 0.7$ , the study of mass-ratio effects on the threshold mass indicated a monotonic relation between the two parameters [87]. A fitting formula for  $M_{\text{thr}}$  dependent on the EOS and the mass-ratio was first derived by Bauswein *et al.* [26], and was shortly followed by an independent study by Kölsch *et al.* [27], who also pointed out that not all EOSs give a monotonically increasing threshold mass with increasing mass ratio. In Ref. [88], Tootle *et al.* were the first to derive a fitting formula for the threshold mass that also includes dependence on the NS spins; we shall not consider the effect of spins in the current work.

For our analysis, we consider the  $M_{\text{thr}}(M_{\text{max}}^{\text{TOV}}, R_{\text{max}}, q)$  fit from Bauswein *et al.* (“Bauswein+ ” from here on), which we denote by

$M_{\text{thr}}^B$  and show explicit expression in Eq. (3.2), and the  $M_{\text{thr}}(M_{\text{max}}^{\text{TOV}}, R_{1.6M_{\odot}}, q)$  fit from Kölsch *et al.* (“Kölsch+” from here on), which we denote by  $M_{\text{thr}}^K$  and show explicit expression in Eq. (3.3). In the above equations,  $M_{\text{max}}^{\text{TOV}}$ ,  $R_{\text{max}}$ ,  $R_{1.6M_{\odot}}$  are maximum mass, radius at the maximum mass and radius at  $1.6 M_{\odot}$  of the non-rotating NS, respectively. We use the Bauswein+ and Kölsch+ numerical fits of  $M_{\text{thr}}$ , as they better capture their NR results, with the exception of

a more fine-tuned fit by Kölsch *et al.* which instead of some fiducial radius, depends on the estimated value of threshold mass at  $q = 1$  (i.e.  $M_{\text{thr}}^{q=1}$ ) based on the NR simulations. However, as  $M_{\text{thr}}^{q=1}$  is a quantity that can only be estimated by NR simulations for a given EOS, we cannot use this fit for our GW170817 analysis, where the EOS is being sampled over; we can only use it in our NR injection studies of Agathos *et al.* [28] (see Sec. IV B). We denote this fit by  $M_{\text{thr}}^{K1}$  and show its explicit expression in Eq. (3.4).

$$M_{\text{thr}}^B(M_{\text{max}}^{\text{TOV}}, R_{\text{max}}, q) = -0.07794 - 5.011(1-q)^3 + [0.1863 - 1.970(1-q)^3] R_{\text{max}} + [0.497 + 11.098(1-q)^3] M_{\text{max}}^{\text{TOV}}, \quad (3.2)$$

$$M_{\text{thr}}^K(M_{\text{max}}^{\text{TOV}}, R_{1.6M_{\odot}}, q) = 0.246 + [0.463 + 0.735(1-q) + 0.172(1-q)^3] M_{\text{max}}^{\text{TOV}} + [0.141 - 0.116(1-q) - 0.214(1-q)^3] R_{1.6M_{\odot}}, \quad (3.3)$$

$$M_{\text{thr}}^{K1}(M_{\text{thr}}^{q=1}, M_{\text{max}}^{\text{TOV}}, q) = 0.281 - [0.03667 - 1.11(1-q) - 1.191(1-q)^3] M_{\text{max}}^{\text{TOV}} + [0.932 - 0.753(1-q) - 1.625(1-q)^3] M_{\text{thr}}^{q=1}. \quad (3.4)$$

We will also compare the predictions of the  $q$ -dependent  $M_{\text{thr}}$  fits listed above with the  $q$ -independent  $M_{\text{thr}}$  fits used in Agathos *et al.*. The latter were derived as a relation between  $k_{\text{thr}}$  and  $C_{\text{max}}$ ,

$$k_{\text{thr}}(C_{\text{max}}) = -(3.29 \pm 0.23)C_{\text{max}} + (2.392 \pm 0.064), \quad (3.5)$$

by combining the results of Refs. [12, 89] with data by the CoRe collaboration [77, 90].

## B. Bayesian analysis of neutron star binaries

We perform Bayesian analysis on the GW detector data using a waveform model with matter effects that depend on the masses and the EOSs, to recover posterior samples of compact binary coalescence (CBC) parameters of the signal GW170817. In addition to the standard CBC parameters for BBH—masses, spins, distance, coalescence time, phase, sky location and orientation angles—we also treat the EOS as an unknown function which we need to sample over. We use the four-dimensional family of EOSs spanned by the spectral parametrization [91–93], where the adiabatic index  $\Gamma$  is approximated by a third-order polynomial  $\Gamma(\rho) = \exp(\sum_{k=0}^3 \gamma_k \log(\rho/p_0))$ . We therefore sample over the additional parameters  $(\gamma_0, \gamma_1, \gamma_2, \gamma_3)$ , to construct the EOS for the NS matter and derive all EoS-dependent parameters, such as tidal deformabilities, NS radii, etc. by solving the TOV equations for the sampled values of  $m_1$  and  $m_2$ .

An obvious benefit of using this method is that for each point in the parameter space of  $(\gamma_0, \gamma_1, \gamma_2, \gamma_3)$ , we can also calculate global properties of the EOS function like  $M_{\text{max}}$ ,  $R_{\text{max}}$ , and  $R_{1.6M_{\odot}}$ . We can then use these

in our fits (Eqs. (3.2), (3.3)), to compute the threshold mass  $M_{\text{thr}}$  for each sample and thus translate the joint posterior of  $(m_1, m_2, \gamma_0, \gamma_1, \gamma_2, \gamma_3)$  to the joint posterior probability of  $(M_{\text{thr}}, M)$ , where  $M$  is the total mass of BNS system.

Finally, we classify each sample to either a formation of a prompt collapse to a BH or a NS remnant (non-prompt collapse), based on whether  $M$  is greater or less than the threshold mass. As the observation of EM counterparts after the observation of the GW170817 signal indicates that it was most likely a non-prompt collapse signal, we can reject a posteriori the part of the BNS parameter space for which we predict a prompt collapse. We can then compare the resulting posteriors with the original results from the LIGO-Virgo analyses [5, 93], and assess the effect of our truncating procedure on measuring the properties of the BNS source.

We repeat the analysis described above by imposing a hard lower bound on the maximum nonrotating TOV mass of the NS EOS, to be consistent with the observation of the binary pulsar J0348+0432 [46]. The measured mass of the pulsar is  $M_{J0348+0432} = 2.01 \pm 0.04 M_{\odot}$ , so we impose a conservative constraint on the maximum TOV mass as  $M_{\text{max}}^{\text{TOV}} \geq 1.97 M_{\odot}$ . This effectively removes a non-negligible part of the EOS parameter space, in particular the subset of models that are too soft to support NSs at masses larger than  $1.97 M_{\odot}$ . In Sec. IV, we will compare the improvement in parameter estimation with and without this constraint.

The IMRPhenomPv2\_NRTidal waveform model was used to measure the source parameters of GW170817 for both the parameter estimation studies of Ref. [5] and the EOS studies of Ref. [93]. The BBH baseline in IMRPhenomPv2\_NRTidal model is based on the point-

particle model presented in Ref. [94], which incorporates effective-one-body (EOB) and NR-tuned tidal effects [95, 96], spin-induced quadrupole effects [97–101] and precession effects. Regarding the matter sector, Ref. [93] makes minimal assumptions about the nature of the source and samples over the tidal deformability parameters in contrast to Ref. [5] where the condition that both NSs in the binary are described by the same EOS is imposed and the 4-dimensional spectral decomposition is used to sample the space of EOSs. The two studies of Refs. [5, 93] also compare the results between different waveform models, namely `SEOBNRv4_ROM_NRTidal` [102], `IMRPhenomD_NRTidal` [103] and `TaylorF2` and found that the systematic uncertainties due to different waveform models are less than the statistical uncertainties in observing GW170817 signal.

### C. Validation of threshold mass fits

In addition to the GW170817 re-analysis, we implement the above Bayesian analysis on the injection study of the BNS systems given in Agathos *et al.* [28]. From the obtained joint posterior probability of  $(M_{\text{thr}}, M)$ , we classify merger outcome into either prompt-collapse to BH or non-prompt collapse, and compute the posterior probability of prompt-collapse, given by

$$P_{\text{PC}} = P(M > M_{\text{thr}} | d, \mathcal{H}_{\text{PC}}), \quad (3.6)$$

for each BNS system of Agathos *et al.*. Here, by  $d$  we denote the simulated data of the detector network (in this case from LIGO Livingston (L1), LIGO Hanford (H1) and Virgo (V1) at design sensitivity), and by  $\mathcal{H}_{\text{PC}}$  we denote the underlying model that we use for estimating the prompt collapse threshold for the total mass. We then also run our above analyses with the additional maximum mass constraint from J0348+0432 and observe the effect this has on the estimate of  $P_{\text{PC}}$ .

The waveform model used for the BNS injection studies of Agathos *et al.* is `TEOBResumS` [79, 104] with the non-spinning tidal model of Ref. [105] and source parameters matching those of the NR simulations, as NR data do not span sufficiently many inspiral cycles to be used for injections. The Bayesian data analysis to recover the source parameters is performed using `TaylorF2` and `IMRPhenomPv2_NRTidal`, restricting to the low-spin prior of [5]. However, as mentioned in Agathos *et al.*, due to an error in the `NRTidal` version used, the `IMRPhenomPv2_NRTidal` analysis led to biases in the tidal deformability inference; we therefore perform our analysis only on their `TaylorF2` results.

## IV. RESULTS

In this Section we discuss our results corresponding to i.) the analysis for the GW170817 event and ii.) the analysis for injection studies of Agathos *et al.* [28].

### A. GW170817 Analysis

We assume that the remnant of GW170817 did not promptly collapse to a black hole and apply our method of Sec. III C at the post-processing level, to the posteriors of the spectral EOS parameters for the two analyses of the GW170817 signal performed in Ref. [93]:

- without maximum mass constraint on  $M_{\text{max}}^{\text{TOV}}$
- with the hard constraint on the maximum mass,  $M_{\text{max}}^{\text{TOV}} > 1.97M_{\odot}$ , consistent with J0348+0432 [46]

We use the two sets of  $q$ -dependent  $M_{\text{thr}}$  fits of Bauswein+ and Kölsch+. For the Kölsch+ fits, however, we only present the analysis for the maximum mass constraint data sample, as the best  $M_{\text{thr}}$  fit given in Ref. [27] is based on the NS radius at  $1.6M_{\odot}$ , i.e.  $R_{1.6M_{\odot}}$ <sup>1</sup>.

We compare the non-prompt collapse subset of the binary parameters like radii ( $r_1, r_2$ ), (dimensionless) tidal deformabilities ( $\Lambda_1, \Lambda_2$ ), mass ratio ( $q$ ), and component masses ( $m_1, m_2$ ) evaluated using the  $M_{\text{thr}}$  fits with the corresponding parameters of the complete LIGO-Virgo data sample. The results of our analysis for GW170817 posteriors for both Bauswein+ and Kölsch+ fits are shown in Fig. 1(a) and 1(b), and Fig. 2, respectively.

Within the 90 % credible limit, we obtain  $m_1 \in (1.37, 1.61)M_{\odot}$ ,  $m_2 \in (1.16, 1.35)M_{\odot}$  for the unconstrained dataset, and  $m_1 \in (1.37, 1.62)M_{\odot}$ ,  $m_2 \in (1.16, 1.35)M_{\odot}$  for the constrained dataset, consistent with the results of Ref. [5]. After removing the prompt collapse cases using Bauswein+ fits (64.80% and 23.04% of the data sample without the constraint and with the constraint, respectively) from the data sample, we obtain the component masses for the remaining non-prompt collapse data sample as  $m_1 \in (1.37, 1.58)M_{\odot}$ ,  $m_2 \in (1.18, 1.36)M_{\odot}$  for the unconstrained dataset, and  $m_1 \in (1.37, 1.60)M_{\odot}$ ,  $m_2 \in (1.17, 1.35)M_{\odot}$  for the constrained dataset, which within the 90% credible limit are also consistent with the results of Ref. [5]. Whereas, after removing the prompt collapse cases using the Kölsch+ fit (14.61% of the data sample) from the constrained dataset, we obtain the component masses for the remaining non-prompt collapse data sample as  $m_1 \in (1.37, 1.59)M_{\odot}$  and  $m_2 \in (1.17, 1.35)M_{\odot}$  are also consistent with the results of Ref. [5] within the 90% credible limit.

For the radii of the two NSs, within the 90 % credible limit, we obtain  $r_1 = 11.2_{-1.5}^{+1.8}$  km,  $r_2 = 11.5_{-1.3}^{+1.6}$  km for the data sample without maximum mass constraint, and  $r_1 = 11.9_{-1.4}^{+1.4}$  km,  $r_2 = 11.9_{-1.3}^{+1.4}$  km for the data sample with maximum mass constrain [28].

<sup>1</sup> That fiducial NS mass is larger than the maximum mass supported by some samples in the unconstrained dataset. Nevertheless, we confirm that after truncating these samples, the resulting posteriors agree well with those derived from the constrained dataset.



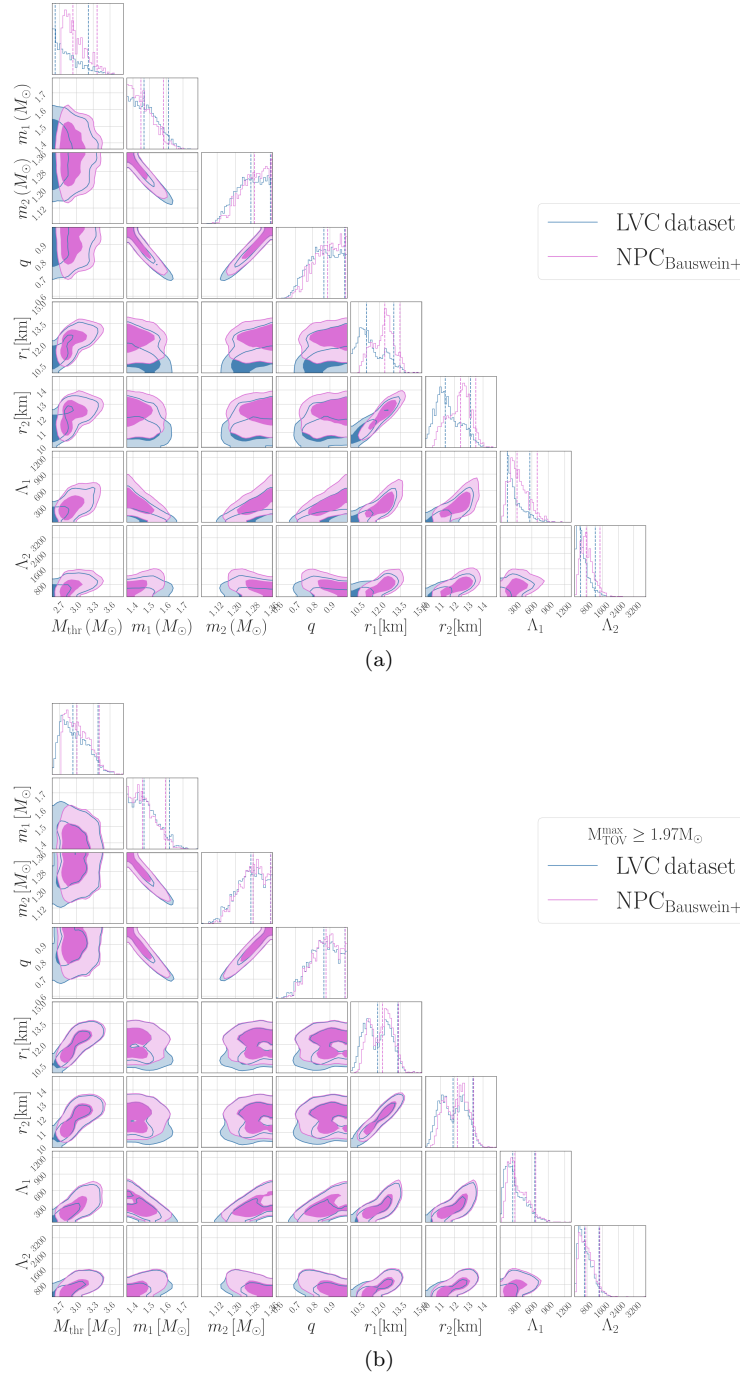


FIG. 1. Corner plot for  $(M_{\text{thr}}, m_1, m_2, \Lambda_1, \Lambda_2, q, r_1, r_2)$  of the GW signal GW1701817 based on the Bauswein+ fit. Blue and purple colors indicate the LIGO-Virgo (LVC) and the corresponding non-prompt collapse (NPC) data samples, respectively. Contours correspond to the 50% and 90% confidence regions for the 2D joint posteriors, whereas in the 1D marginalized posteriors dotted lines show the 90% credible interval for each parameter. The plots correspond to (a): the data sample without maximum mass constraint, and (b): the data sample with a hard lower bound on maximum mass at  $1.97 M_\odot$ .

Hence, we see that the maximum mass constraint rules out the possibility of radii  $< 10$  km compared to the data sample without maximum mass constraint. This is due to the fact that the soft EOSs that predict low NS radii do not support massive NSs. For the non-prompt col-

lapse data sample based on the Bauswein+ fit, we obtain  $r_1 = 12.3^{+1.2}_{-1.3}$  km,  $r_2 = 12.3^{+1.2}_{-1.4}$  km for the unconstrained dataset and  $r_1 = 12.1^{+1.3}_{-1.2}$  km,  $r_2 = 12.1^{+1.2}_{-1.2}$  km for the constrained dataset. This shows that under the non-

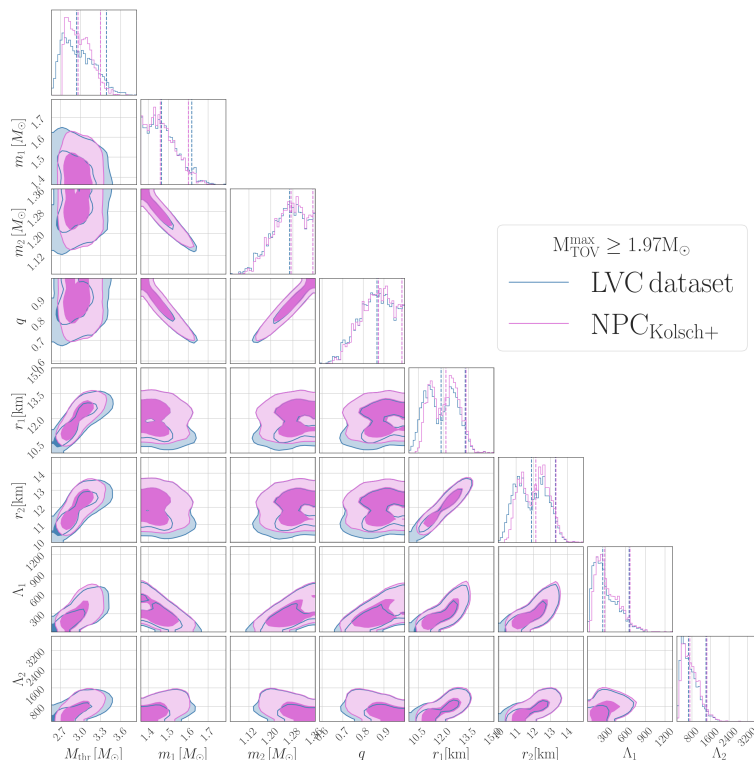


FIG. 2. Same as Fig. 1, but using the K lsch+ fit; both datasets are generated using the hard lower bound on the maximum mass at  $1.97M_\odot$ .

prompt-collapse hypothesis, based on the  $q$ -dependent Bauswein+ fit, our GW analysis alone already rules out the possibility of NS radii  $< 10\text{km}$ , even without using observations of heavy NSs.

Based on the K lsch+ fit, the radii of the two NSs within 90% credible limit for the non-prompt collapse dataset are now  $r_1 = 12.1^{+1.2}_{-1.2}\text{ km}$  and  $r_2 = 12.1^{+1.2}_{-1.3}\text{ km}$ . The K lsch+ fit also rules out radii  $< 10\text{km}$  consistent with the findings of Refs. [5, 28] for the constrained dataset, as well as with the  $R_{1.6}$  bound of Ref. [24]. Additionally, we observe an improvement in the radii constraints as the uncertainty of NS radii decreases for the non-prompt collapse data samples. The uncertainty in NS radii for the unconstrained LVC dataset decreases from 3.3 km to 2.6 km after removing the prompt collapse cases using the Bauswein+ fit. Similarly, the uncertainty in NS radii for the constrained LVC dataset decreases from 2.8 km to 2.5 km for Bauswein+ and K lsch+ fits, based on non-prompt-collapse data samples. This improvement in constraints on the radii implies improved constraints on the EOSs of the NS.

To illustrate the impact of our analysis, we plot the mass-radius curve for the posterior of the GW170817 signal along with the mass-radius curve for the selected EOSs (WFF1, APR4, SLy, MPA1, H4) in Figs. 3(a) and 3(b). Within the 90% credible limit, the EOSs consistent with the NPC dataset are only APR4, SLy, and MPA1, compared to the complete LVC dataset that was also

supporting WFF1.

This follows from the improvement in the NS radii measurements, both in the case of the unconstrained dataset using the Bauswein+ fit for  $M_{\text{thr}}$ , and in the cases of the constrained dataset using either the Bauswein+ fit or the K lsch+ fit.

Overall, we observe that the effect of using a  $q$ -dependent classification of the remnant improves our constraints on the NS EOS and radii in much the same way as a maximum mass constraint does, i.e. by excluding part of the soft-EOS corner of the parameter space. In this particular case, the effect of using the non-prompt-collapse hypothesis is stronger than the effect of imposing a maximum mass constraint at  $1.97M_\odot$ , as highlighted in Fig. 3.

## B. Injection studies

To check the robustness of the Bauswein+ and K lsch+ fits, we use progenitor and remnant information from the existing NR simulations of BNS mergers given in Agathos *et al.* [28]. We generate posteriors of CBC parameters using the TaylorF2 waveform model for each of these BNS systems. Similar to the GW170817 analysis of Sec. IV A, we consider the two cases of the BNSs, i.e. constrained and unconstrained datasets with respect to the maximum NS mass. After classifying the

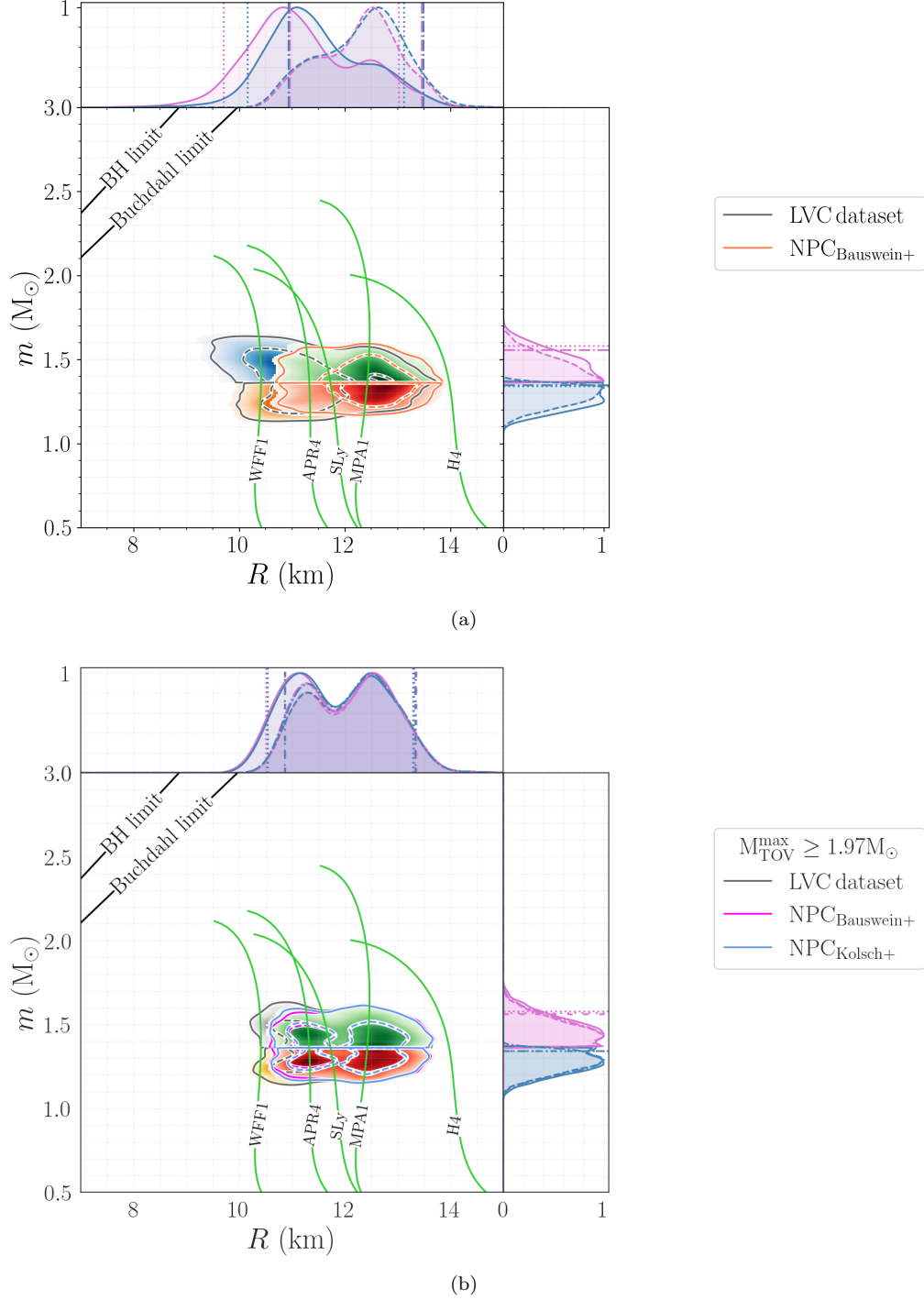


FIG. 3. Mass-Radius posterior plots for the mass ‘ $m$ ’ and radius ‘ $R$ ’ of each binary component of GW signal GW170817 for both (a): the data sample without the maximum mass constraint, and (b): the data sample with the hard constraint on maximum mass,  $M_{\text{max}}^{\text{TOV}} > 1.97 M_{\odot}$ , corresponding to observation of binary pulsar J0348+0432. The black solid lines in top left indicates the Schwarzschild limit ( $R = 2m$ ), and the Buchdahl limit ( $R = \frac{9}{4}m$ ). Mass-Radius curves of selected EOSs are plotted in green color. In the one-dimensional plots, solid and dotted lines indicate the LIGO-Virgo (LVC) data sample and its 90 % credible limit bounds, respectively, and dashed and dashdotted lines indicate the corresponding non-prompt collapse (NPC) data sample and its the 90 % credible limit bounds, respectively.

merger remnant of each dataset using the above fits for the threshold mass, we calculate the cumulative probability distribution of prompt collapse,  $P(M > M_{\text{thr}})$ .

Here too, for the Kölsch+ fit we only calculate the cumulative probability of prompt collapse for the constrained dataset. The cumulative probability distribution (CDF) plots for the constrained dataset using the Bauswein+ and Kölsch+ fits are shown in Fig. 4(a) and Fig. 4(b), respectively<sup>2</sup>. The vertical line in the plot corresponds to the threshold of prompt collapse (beyond which the total mass exceeds the threshold mass). We observe that the  $q$ -dependent Bauswein+ and Kölsch+ fits correctly infer the merger outcome for most of the BNS models except for a few cases, all of which were also misclassified in Agathos *et al.*

Then we compare the probability of prompt collapse predicted by the  $q$ -dependent Bauswein+ and Kölsch+ fits with the one by the  $q$ -independent  $M_{\text{thr}}$  fit of Agathos *et al.* (see, Eq. (3.5) for the fit formula). The summary of the results based on these fit formulae along with the binary parameters and the outcome of the merger for each BNS is shown in Table I. We observe that both Bauswein+ and Kölsch+ fits better capture the formation of prompt-collapse to a BH as the probability for prompt-collapse increases for both the cases of data samples compared to  $q$ -independent  $M_{\text{thr}}$  fit of Agathos *et al.* Furthermore, we observe that compared to Bauswein+ , the Kölsch+ fit is better at predicting the type of merger remnant, as it typically gives higher probabilities when a prompt collapse does occur and lower probabilities in the cases resulting to a (meta-)stable remnant. We see that even for the few cases where the merger remnant is misclassified (SFHo 1.4 + 1.4, ALF2 1.5 + 1.5), with respect to the results of Agathos *et al.*, the probability of prompt collapse has significantly moved towards the correct direction.

Finally, as mentioned in Sec. III A, we also use the  $M_{\text{thr}}^{K1}$  fit [27] dependent on the estimated value of the threshold mass at ( $q = 1$ ) from NR simulation data (i.e.,  $M_{\text{thr}}^{q=1}$ ), together with  $M_{\text{max}}^{\text{TOV}}$  and  $q$  for our analysis (see Eq. (3.4) for the fitting formula). The values of the threshold mass at ( $q = 1$ ) for the EOSs of interest are obtained from the NR data of Refs. [25, 27, 28, 47] (see, Table II). The probability of prompt collapse computed corresponding to this fit is given in Table I. From Table I, we see that this fit better captures both the formation of a prompt collapse to a BH and a non-prompt collapse compared to all other  $M_{\text{thr}}$  fits considered in our analysis for most of the BNS systems; however, it is only available for a small discrete set of EOSs.

## V. CONCLUSIONS

We analyse the gravitational wave signal GW170817 using the  $q$ -dependent threshold mass fits given in Bauswein *et al.* [26] and Kölsch *et al.* [27]. For our analysis, we consider the two cases of GW170817 signal - without the maximum mass constraint data sample and with the hard constraint on the maximum mass data sample corresponding to the observation of binary pulsar J0348+0432. Using the threshold mass fits we identify the prompt collapse cases which we then remove from the two data samples for our analysis. Then we compare the non-prompt collapse data sample of each case with its corresponding LVC data sample. We observe that the non-prompt collapse data sample removes the radii  $< 10$  km even for without the maximum mass constraint data sample in comparison to results observed in Refs. [5, 28] where radii  $< 10$  km is not supported only by the data sample with the maximum mass constraint. We also see that for the non-prompt collapse data sample the uncertainty of NS radii decreases implying improved constraints on the NS radii and hence the EOSs. As an example, we observe that the EOS WFF1 is not supported by the non-prompt collapse data sample for both the cases of GW170817 signal compared to the results of Refs. [5, 28].

The threshold mass fits are then validated with a set of 17 injections given in Agathos *et al.* [28]. The merger remnant for all the signals are not just correctly inferred from both fits but the probability of the formation of a prompt collapse is also improved compared to the  $q$ -independent fit of Agathos *et al.* with the exception of a few signals. Additionally, we observe that the probability of formation of both a prompt collapse and a non-prompt collapse remnant has improved for  $q$ -dependent threshold mass fits of Kölsch *et al.* compared to both the fits of Bauswein *et al.* and Agathos *et al.*

Application of either of the fits, Bauswein+ or Kölsch+ to the GW170817 analysis gives similar improvements for the posterior PDFs of NS masses and radii. This suggests that any differences between these two fits have relatively small impact for GW170817-like signals, that should also allow us to improve the constraints on the NS properties for similar detections in the future. Nevertheless, the BNS parameter space, especially in the regions close to the prompt-collapse threshold, need to be explored more densely with future numerical relativity simulations, for a variety of EOSs.

## ACKNOWLEDGMENTS

The authors are grateful to Ulrich Sperhake, Sebastiano Bernuzzi and Alessandro Nagar for useful discussions during the preparation of this work and to Nikolaos Stergioulas for reviewing the manuscript and providing useful comments. T.J. is jointly funded by the Cambridge Trust, Department of Applied Mathematics

<sup>2</sup> For the unconstrained dataset CDFs with the Bauswein+ fit, see Fig. 5 in Appendix A.



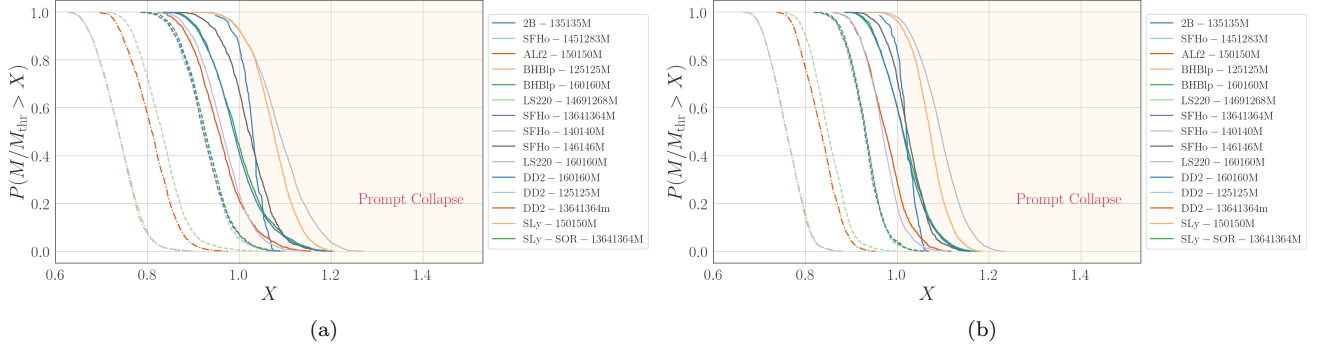


FIG. 4. Cumulative probability of  $M/M_{\text{thr}}$ , the ratio between total mass ( $M$ ) and the threshold mass ( $M_{\text{thr}}$ ), for the injection study using the simulated BNS systems of Table I with a hard lower bound on maximum mass at  $1.97M_{\odot}$ . The probability of prompt collapse for each binary neutron star system is at  $X = 1$ . The solid, dashed and dashed-dotted lines correspond to formation of a BH, HMNS, and MNS, respectively. The plots correspond to (a): Bauswein+ fit of Eq. (3.2), and (b): Kölsch+ fit of Eq. (3.3), respectively.

TABLE I. Summary of probability of prompt collapse (%) for the known inspiral-merger waveforms of Agathos *et al.* [28]. The collapse time  $t_{\text{BH}}$  is time measured from the peak of GW amplitude, called the merger time. The threshold mass fit formulas  $M_{\text{thr}}(M_{\text{max}}^{\text{TOV}}, C_{\text{max}})$ ,  $M_{\text{thr}}(M_{\text{max}}^{\text{TOV}}, R_{\text{max}}, q)$ ,  $M_{\text{thr}}(M_{\text{max}}, R_{1.6M_{\odot}}, q)$ , and  $M_{\text{thr}}(M_{\text{max}}^{\text{TOV}}, M_{\text{thr}, (q=1)}, q)$  are given in Eqs. (3.2)-(3.5), respectively.

EOS	$m_1(\text{M}_{\odot})$	$m_2(\text{M}_{\odot})$	$t_{\text{BH}}[\text{ms}]$	Remnant at $t \sim 3\text{ms}$	$M_{\text{thr}}(M_{\text{max}}^{\text{TOV}}, C_{\text{max}})$ Agathos <i>et al.</i> [28]	$M_{\text{thr}}(M_{\text{max}}^{\text{TOV}}, R_{\text{max}}, q)$ Bauswein <i>et al.</i> [26]	$M_{\text{thr}}(M_{\text{max}}^{\text{TOV}}, R_{1.6\text{M}_{\odot}}, q)$ Kölsch <i>et al.</i> [27]	$M_{\text{thr}}(M_{\text{max}}^{\text{TOV}}, M_{\text{thr}}^{q=1}, q)$ Kölsch <i>et al.</i> [27]		
					$P_{\text{PC}}^{\text{M}_{\text{thr}}}$	$P_{\text{PC}}^{\text{M}_{\text{thr}}, \text{M}_{\text{max}}^{\text{TOV}}}$	$P_{\text{PC}}^{\text{M}_{\text{thr}}}$	$P_{\text{PC}}^{\text{M}_{\text{thr}}, \text{M}_{\text{max}}^{\text{TOV}}}$	$P_{\text{PC}}^{\text{M}_{\text{thr}}, \text{M}_{\text{max}}^{\text{TOV}}}$	$P_{\text{PC}}^{\text{M}_{\text{thr}}, \text{M}_{\text{max}}^{\text{TOV}}}$
2B	1.35	1.35	0.49	BH	99.5	67.1	99.9	86.3	83.6	100.0
SFHo	1.40	1.40	1.07	BH	46.7	8.0	58.8	23.6	18.8	17.6
SFHo	1.46	1.46	0.70	BH	77.2	48.1	85.6	66.5	71.5	100.0
ALF2	1.50	1.50	0.64	BH	25.7	5.7	36.6	21.1	28.6	84.0
BHBA $\phi$	1.60	1.60	0.99	BH	40.7	27.2	53.4	44.0	60.1	100.0
LS220	1.60	1.60	0.63	BH	92.4	88.1	95.3	92.6	97.9	100.0
DD2	1.60	1.60	$\sim 3$	BH	37.7	24.2	50.2	40.9	59.7	32.0
SLy	1.50	1.50	0.99	BH	96.1	87.9	97.6	92.5	96.2	100.0
SFHo	1.364	1.364	$\sim 4$	HMNS	25.7	0.5	34.1	6.7	4.0	3.4
SLy-SOR	1.364	1.364	$\sim 14$	HMNS	29.8	0.6	39.1	7.2	3.4	4.8
SFHo	1.45	1.283	$\sim 12$	HMNS	25.9	0.4	34.7	5.0	2.7	2.9
LS220	1.469	1.268	$\sim 33$	HMNS	0.8	0.0	1.9	0.4	0.0	0.1
BHBA $\phi$	1.25	1.25	$>20$	MNS	0.0	0.0	0.0	0.0	0.0	0.0
DD2	1.25	1.25	$>20$	MNS	0.0	0.0	0.0	0.0	0.0	0.0
DD2	1.364	1.364	$\sim 21$	MNS	0.1	0.0	0.9	0.0	0.0	0.0

TABLE II. NR simulation based values of  $M_{\text{thr}}^{q=1}$  for EOSs considered in Agathos *et al.* [28].

EOS	$M_{\text{thr}}^{q=1}$	Reference
2B	2.43	[28]
SFHo	2.824	[25, 47]
ALF2	2.963	[27]
BHBA $\phi$	3.024	[25, 47]
LS220	2.956	[25, 47]
DD2	3.274	[25, 47]
SLy	2.756	[27]

and Theoretical Physics (DAMTP), and Centre for Doctoral Training, University of Cambridge. M.A. is supported by the Kavli Foundation. This material is based upon work supported by NSF's LIGO Laboratory which is a major facility fully funded by the National Science Foundation. This work makes use of GNU Scientific Library, NumPy [106], SciPy [107], Matplotlib [108], seaborn [109] and LALsuite [110, 111] software packages.

## Appendix A: Effect of $M_{\text{max}}^{\text{TOV}}$ constraint

In this Appendix, we analyse the impact of the maximum mass constraint corresponding to the observation of binary pulsar J0348+0432 on the known BNS inspiral-merger waveforms of Agathos *et al.* [28]. For this, we first calculate the cumulative probability of prompt collapse [ $P(M > M_{\text{thr}})$ ] for the unconstrained dataset and then compare it with the results presented in Fig. 4(a). The cumulative probability plot for the data sample without maximum mass constraint is shown in Fig. 5.

On comparing Fig. 5 with Fig. 4(a), we observe that ratio  $M/M_{\text{thr}}$  decreases for the constrained dataset compared to the unconstrained dataset. This can be due to increase in the  $M_{\text{thr}}$  values, which is expected, as the maximum mass constraint removes the soft part of the EOSs. This is also reflected from the results in Table I, where we see a decreasing trend in the probability of prompt collapse for the constrained dataset compared to the unconstrained dataset.

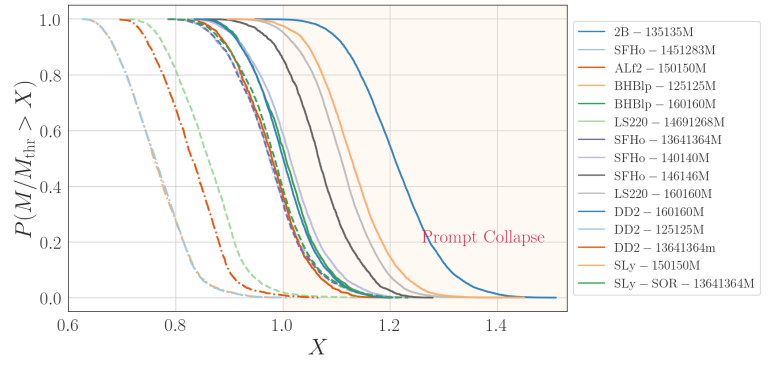


FIG. 5. Cumulative probability of  $M/M_{\text{thr}}$ , the ratio between total mass ( $M$ ) and the threshold mass ( $M_{\text{thr}}$ ), for the injection study using simulated BNS systems of Table I for ‘Bauswein+’ fit of Eq. (3.2). The probability of prompt collapse for each binary neutron star system is at  $X = 1$ . The solid, dashed and dashed-dotted lines correspond to formation of a BH, HMNS, and MNS, respectively.

- 
- [1] B. P. Abbott *et al.* (LIGO Scientific, Virgo), Observation of Gravitational Waves from a Binary Black Hole Merger, *Phys. Rev. Lett.* **116**, 061102 (2016), [arXiv:1602.03837 \[gr-qc\]](#).
  - [2] J. Aasi *et al.* (LIGO Scientific), Advanced LIGO, *Class. Quant. Grav.* **32**, 074001 (2015), [arXiv:1411.4547 \[gr-qc\]](#).
  - [3] F. Acernese *et al.* (VIRGO), Advanced Virgo: a second-generation interferometric gravitational wave detector, *Class. Quant. Grav.* **32**, 024001 (2015), [arXiv:1408.3978 \[gr-qc\]](#).
  - [4] B. P. Abbott *et al.* (LIGO Scientific, Virgo), GW170817: Observation of Gravitational Waves from a Binary Neutron Star Inspiral, *Phys. Rev. Lett.* **119**, 161101 (2017), [arXiv:1710.05832 \[gr-qc\]](#).
  - [5] B. P. Abbott *et al.* (LIGO Scientific, Virgo), Properties of the binary neutron star merger GW170817, *Phys. Rev. X* **9**, 011001 (2019), [arXiv:1805.11579 \[gr-qc\]](#).
  - [6] B. P. Abbott *et al.* (LIGO Scientific, Virgo), GWTC-1: A Gravitational-Wave Transient Catalog of Compact Binary Mergers Observed by LIGO and Virgo during the First and Second Observing Runs, *Phys. Rev. X* **9**, 031040 (2019), [arXiv:1811.12907 \[astro-ph.HE\]](#).
  - [7] B. P. Abbott *et al.* (LIGO Scientific, Virgo), GW190425: Observation of a Compact Binary Coalescence with Total Mass  $\sim 3.4M_{\odot}$ , *Astrophys. J. Lett.* **892**, L3 (2020), [arXiv:2001.01761 \[astro-ph.HE\]](#).
  - [8] M. Shibata, Constraining nuclear equations of state using gravitational waves from hypermassive neutron stars, *Phys. Rev. Lett.* **94**, 201101 (2005), [arXiv:gr-qc/0504082](#).
  - [9] M. Shibata and K. Taniguchi, Merger of binary neutron stars to a black hole: disk mass, short gamma-ray bursts, and quasinormal mode ringing, *Phys. Rev. D* **73**, 064027 (2006), [arXiv:astro-ph/0603145](#).
  - [10] L. Baiotti, B. Giacomazzo, and L. Rezzolla, Accurate evolutions of inspiralling neutron-star binaries: prompt and delayed collapse to black hole, *Phys. Rev. D* **78**, 084033 (2008), [arXiv:0804.0594 \[gr-qc\]](#).
  - [11] K. Hotokezaka, K. Kyutoku, H. Okawa, M. Shibata, and K. Kiuchi, Binary Neutron Star Mergers: Dependence on the Nuclear Equation of State, *Phys. Rev. D* **83**, 124008 (2011), [arXiv:1105.4370 \[astro-ph.HE\]](#).
  - [12] A. Bauswein, T. W. Baumgarte, and H. T. Janka, Prompt merger collapse and the maximum mass of neutron stars, *Phys. Rev. Lett.* **111**, 131101 (2013), [arXiv:1307.5191 \[astro-ph.SR\]](#).
  - [13] A. Bauswein and N. Stergioulas, Semi-analytic derivation of the threshold mass for prompt collapse in binary neutron star mergers, *Mon. Not. Roy. Astron. Soc.* **471**, 4956 (2017), [arXiv:1702.02567 \[astro-ph.HE\]](#).
  - [14] S. Bernuzzi, Neutron Star Merger Remnants, *Gen. Rel. Grav.* **52**, 108 (2020), [arXiv:2004.06419 \[astro-ph.HE\]](#).
  - [15] B. P. Abbott *et al.* (LIGO Scientific, Virgo, Fermi-GBM, INTEGRAL), Gravitational Waves and Gamma-rays from a Binary Neutron Star Merger: GW170817 and GRB 170817A, *Astrophys. J. Lett.* **848**, L13 (2017), [arXiv:1710.05834 \[astro-ph.HE\]](#).
  - [16] E. Troja *et al.*, The X-ray counterpart to the gravitational wave event GW 170817, *Nature* **551**, 71 (2017), [arXiv:1710.05433 \[astro-ph.HE\]](#).
  - [17] B. P. Abbott *et al.* (LIGO Scientific, Virgo, Fermi-GBM, INTEGRAL, IceCube, AstroSat Cadmium Zinc Telluride Imager Team, IPN, Insight-Hxmt, ANTARES, Swift, AGILE Team, 1M2H Team, Dark Energy Camera GW-EM, DES, DLT40, GRAWITA, Fermi-LAT, ATCA, ASKAP, Las Cumbres Observatory Group, OzGrav, DWF (Deeper Wider Faster Program), AST3, CAASTRO, VINROUGE, MASTER, J-GEM, GROWTH, JAGWAR, CaltechNRAO, TTU-NRAO, NuSTAR, Pan-STARRS, MAXI Team, TZAC Consortium, KU, Nordic Optical Telescope,

- ePESSTO, GROND, Texas Tech University, SALT Group, TOROS, BOOTES, MWA, CALET, IKI-GW Follow-up, H.E.S.S., LOFAR, LWA, HAWC, Pierre Auger, ALMA, Euro VLBI Team, Pi of Sky, Chandra Team at McGill University, DFN, ATLAS Telescopes, High Time Resolution Universe Survey, RIMAS, RATIR, SKA South Africa/MeerKAT), Multi-messenger Observations of a Binary Neutron Star Merger, *Astrophys. J. Lett.* **848**, L12 (2017), [arXiv:1710.05833 \[astro-ph.HE\]](#).
- [18] M. Tanaka *et al.*, Kilonova from post-merger ejecta as an optical and near-infrared counterpart of GW170817, *Publ. Astron. Soc. Jap.* **69**, psx12 (2017), [arXiv:1710.05850 \[astro-ph.HE\]](#).
- [19] N. R. Tanvir *et al.*, The Emergence of a Lanthanide-Rich Kilonova Following the Merger of Two Neutron Stars, *Astrophys. J. Lett.* **848**, L27 (2017), [arXiv:1710.05455 \[astro-ph.HE\]](#).
- [20] P. S. Cowperthwaite *et al.*, The Electromagnetic Counterpart of the Binary Neutron Star Merger LIGO/Virgo GW170817. II. UV, Optical, and Near-infrared Light Curves and Comparison to Kilonova Models, *Astrophys. J. Lett.* **848**, L17 (2017), [arXiv:1710.05840 \[astro-ph.HE\]](#).
- [21] M. Nicholl *et al.*, The Electromagnetic Counterpart of the Binary Neutron Star Merger LIGO/VIRGO GW170817. III. Optical and UV Spectra of a Blue Kilonova From Fast Polar Ejecta, *Astrophys. J. Lett.* **848**, L18 (2017), [arXiv:1710.05456 \[astro-ph.HE\]](#).
- [22] R. Chornock *et al.*, The Electromagnetic Counterpart of the Binary Neutron Star Merger LIGO/VIRGO GW170817. IV. Detection of Near-infrared Signatures of r-process Nucleosynthesis with Gemini-South, *Astrophys. J. Lett.* **848**, L19 (2017), [arXiv:1710.05454 \[astro-ph.HE\]](#).
- [23] D. A. Coulter *et al.*, Swope Supernova Survey 2017a (SSS17a), the Optical Counterpart to a Gravitational Wave Source, *Science* **358**, 1556 (2017), [arXiv:1710.05452 \[astro-ph.HE\]](#).
- [24] A. Bauswein, O. Just, H.-T. Janka, and N. Stergioulas, Neutron-star radius constraints from GW170817 and future detections, *Astrophys. J. Lett.* **850**, L34 (2017), [arXiv:1710.06843 \[astro-ph.HE\]](#).
- [25] R. Kashyap *et al.*, Numerical relativity simulations of prompt collapse mergers: Threshold mass and phenomenological constraints on neutron star properties after GW170817, *Phys. Rev. D* **105**, 103022 (2022), [arXiv:2111.05183 \[astro-ph.HE\]](#).
- [26] A. Bauswein, S. Blacker, G. Lioutas, T. Soutanis, V. Vijayan, and N. Stergioulas, Systematics of prompt black-hole formation in neutron star mergers, *Phys. Rev. D* **103**, 123004 (2021), [arXiv:2010.04461 \[astro-ph.HE\]](#).
- [27] M. Kölsch, T. Dietrich, M. Ujevic, and B. Bruegmann, Investigating the mass-ratio dependence of the prompt-collapse threshold with numerical-relativity simulations, *Phys. Rev. D* **106**, 044026 (2022), [arXiv:2112.11851 \[gr-qc\]](#).
- [28] M. Agathos, F. Zappa, S. Bernuzzi, A. Perego, M. Breschi, and D. Radice, Inferring Prompt Black-Hole Formation in Neutron Star Mergers from Gravitational-Wave Data, *Phys. Rev. D* **101**, 044006 (2020), [arXiv:1908.05442 \[gr-qc\]](#).
- [29] S. Bernuzzi and D. Hilditch, Constraint violation in free evolution schemes: Comparing BSSNOK with a conformal decomposition of Z4, *Phys. Rev. D* **81**, 084003 (2010), [arXiv:0912.2920 \[gr-qc\]](#).
- [30] D. Hilditch, S. Bernuzzi, M. Thierfelder, Z. Cao, W. Tichy, and B. Bruegmann, Compact binary evolutions with the Z4c formulation, *Phys. Rev. D* **88**, 084057 (2013), [arXiv:1212.2901 \[gr-qc\]](#).
- [31] J. R. van Meter, J. G. Baker, M. Koppitz, and D.-I. Choi, How to move a black hole without excision: Gauge conditions for the numerical evolution of a moving puncture, *Physical Review D* **73**, 10.1103/physrevd.73.124011 (2006).
- [32] M. Alcubierre, B. Bruegmann, P. Diener, M. Koppitz, D. Pollney, E. Seidel, and R. Takahashi, Gauge conditions for long term numerical black hole evolutions without excision, *Phys. Rev. D* **67**, 084023 (2003), [arXiv:gr-qc/0206072](#).
- [33] C. Bona, J. Massó, J. Stela, and E. Seidel, *A class of hyperbolic gauge conditions*, in *The Seventh Marcel Grossmann Meeting: On Recent Developments in Theoretical and Experimental General Relativity, Gravitation, and Relativistic Field Theories*, edited by R. T. Jantzen, G. C. Keiser, and R. Ruffini (WORLD SCIENTIFIC, 1997).
- [34] R. Oechslin, S. Rosswog, and F. K. Thielemann, Conformally flat smoothed particle hydrodynamics: application to neutron star mergers, *Phys. Rev. D* **65**, 103005 (2002), [arXiv:gr-qc/0111005](#).
- [35] R. Oechslin, H. T. Janka, and A. Marek, Relativistic neutron star merger simulations with non-zero temperature equations of state. 1. Variation of binary parameters and equation of state, *Astron. Astrophys.* **467**, 395 (2007), [arXiv:astro-ph/0611047](#).
- [36] A. Bauswein, H. T. Janka, and R. Oechslin, Testing Approximations of Thermal Effects in Neutron Star Merger Simulations, *Phys. Rev. D* **82**, 084043 (2010), [arXiv:1006.3315 \[astro-ph.SR\]](#).
- [37] J. Isenberg and J. Nester, *General Relativity and Gravitation*, p. 23 (Plenum Press, New York, 1980).
- [38] J. R. Wilson, G. J. Mathews, and P. Marronetti, Relativistic numerical model for close neutron star binaries, *Phys. Rev. D* **54**, 1317 (1996), [arXiv:gr-qc/9601017](#).
- [39] J. J. Monaghan, Smoothed particle hydrodynamics, *Annual Review of Astronomy and Astrophysics* **30**, 543 (1992), <https://doi.org/10.1146/annurev.aa.30.090192.002551>.
- [40] R. Hockney and J. Eastwood, *Computer Simulation Using Particles (1st ed.)* (CRC Press, 1988).
- [41] M. J. Berger and J. Olinger, Adaptive mesh refinement for hyperbolic partial differential equations, *Journal of Computational Physics* **53**, 484 (1984).
- [42] R. Hess, *Dynamically Adaptive Multigrid on Parallel Computers for a Semi-Implicit Discretization of the Shallow Water Equations* (GMD Forschungszentrum Informationstechnik GmbH, St. Augustin, Germany, 1999).
- [43] M. Alford, M. Braby, M. W. Paris, and S. Reddy, Hybrid stars that masquerade as neutron stars, *Astrophys. J.* **629**, 969 (2005), [arXiv:nucl-th/0411016](#).
- [44] F. Douchin and P. Haensel, A unified equation of state of dense matter and neutron star structure, *Astron. Astrophys.* **380**, 151 (2001), [arXiv:astro-ph/0111092](#).
- [45] B. D. Lackey, M. Nayyar, and B. J. Owen, Observational constraints on hyperons in neutron stars, *Phys. Rev. D* **73**, 024021 (2006), [arXiv:astro-ph/0507312](#).

- [46] J. Antoniadis *et al.*, A Massive Pulsar in a Compact Relativistic Binary, *Science* **340**, 6131 (2013), [arXiv:1304.6875 \[astro-ph.HE\]](#).
- [47] A. Perego, D. Logoteta, D. Radice, S. Bernuzzi, R. Kashyap, A. Das, S. Padamata, and A. Prakash, Probing the incompressibility of nuclear matter at ultra-high density through the prompt collapse of asymmetric neutron star binaries, (2021), [arXiv:2112.05864 \[astro-ph.HE\]](#).
- [48] S. Banik, M. Hempel, and D. Bandyopadhyay, New Hyperon Equations of State for Supernovae and Neutron Stars in Density-dependent Hadron Field Theory, *Astrophys. J. Suppl.* **214**, 22 (2014), [arXiv:1404.6173 \[astro-ph.HE\]](#).
- [49] M. Fortin, M. Oertel, and C. Providência, Hyperons in hot dense matter: what do the constraints tell us for equation of state?, *Publications of the Astronomical Society of Australia* **35**, e044 (2018).
- [50] M. Marques, M. Oertel, M. Hempel, and J. Novak, New temperature dependent hyperonic equation of state: Application to rotating neutron star models and  $I$ - $Q$  relations, *Phys. Rev. C* **96**, 045806 (2017), [arXiv:1706.02913 \[nucl-th\]](#).
- [51] M. Hempel and J. Schaffner-Bielich, Statistical Model for a Complete Supernova Equation of State, *Nucl. Phys. A* **837**, 210 (2010), [arXiv:0911.4073 \[nucl-th\]](#).
- [52] S. Typel, G. Ropke, T. Klähn, D. Blaschke, and H. H. Wolter, Composition and thermodynamics of nuclear matter with light clusters, *Phys. Rev. C* **81**, 015803 (2010), [arXiv:0908.2344 \[nucl-th\]](#).
- [53] S. Typel, Relativistic model for nuclear matter and atomic nuclei with momentum-dependent self-energies, *Phys. Rev. C* **71**, 064301 (2005), [arXiv:nucl-th/0501056](#).
- [54] D. Alvarez-Castillo, A. Ayriyan, S. Benic, D. Blaschke, H. Grigorian, and S. Typel, New class of hybrid EoS and Bayesian M-R data analysis, *Eur. Phys. J. A* **52**, 69 (2016), [arXiv:1603.03457 \[nucl-th\]](#).
- [55] A. Akmal, V. R. Pandharipande, and D. G. Ravenhall, The Equation of state of nucleon matter and neutron star structure, *Phys. Rev. C* **58**, 1804 (1998), [arXiv:nucl-th/9804027](#).
- [56] S. Goriely, N. Chamel, and J. M. Pearson, Further explorations of Skyrme-Hartree-Fock-Bogoliubov mass formulas. XII: Stiffness and stability of neutron-star matter, *Phys. Rev. C* **82**, 035804 (2010), [arXiv:1009.3840 \[nucl-th\]](#).
- [57] R. B. Wiringa, V. Fiks, and A. Fabrocini, Equation of state for dense nucleon matter, *Phys. Rev. C* **38**, 1010 (1988).
- [58] J. M. Lattimer and F. Douglas Swesty, A generalized equation of state for hot, dense matter, *Nuclear Physics A* **535**, 331 (1991).
- [59] G. Shen, C. J. Horowitz, and S. Teige, A New Equation of State for Astrophysical Simulations, *Phys. Rev. C* **83**, 035802 (2011), [arXiv:1101.3715 \[astro-ph.SR\]](#).
- [60] G. A. Lalazissis, J. König, and P. Ring, A New parametrization for the Lagrangian density of relativistic mean field theory, *Phys. Rev. C* **55**, 540 (1997), [arXiv:nucl-th/9607039](#).
- [61] M. Hempel, T. Fischer, J. Schaffner-Bielich, and M. Liebendorfer, New Equations of State in Simulations of Core-Collapse Supernovae, *Astrophys. J.* **748**, 70 (2012), [arXiv:1108.0848 \[astro-ph.HE\]](#).
- [62] A. W. Steiner, M. Hempel, and T. Fischer, Core-collapse supernova equations of state based on neutron star observations, *Astrophys. J.* **774**, 17 (2013), [arXiv:1207.2184 \[astro-ph.SR\]](#).
- [63] H. Mütter, M. Prakash, and T. L. Ainsworth, The nuclear symmetry energy in relativistic Brueckner-Hartree-Fock calculations, *Phys. Lett. B* **199**, 469 (1987).
- [64] L. Engvik, G. Bao, M. Hjorth-Jensen, E. Osnes, and E. Ostgaard, Asymmetric nuclear matter and neutron star properties, *Astrophys. J.* **469**, 794 (1996), [arXiv:nucl-th/9509016](#).
- [65] A. S. Schneider, C. Constantinou, B. Muccioli, and M. Prakash, Akmal-Pandharipande-Ravenhall equation of state for simulations of supernovae, neutron stars, and binary mergers, *Phys. Rev. C* **100**, 025803 (2019), [arXiv:1901.09652 \[nucl-th\]](#).
- [66] J. S. Read, B. D. Lackey, B. J. Owen, and J. L. Friedman, Constraints on a phenomenologically parameterized neutron-star equation of state, *Phys. Rev. D* **79**, 124032 (2009), [arXiv:0812.2163 \[astro-ph\]](#).
- [67] N. K. Glendenning, Neutron Stars Are Giant Hypernuclei?, *Astrophys. J.* **293**, 470 (1985).
- [68] Y. Sugahara and H. Toki, Relativistic mean field theory for unstable nuclei with nonlinear sigma and omega terms, *Nucl. Phys. A* **579**, 557 (1994).
- [69] H. Toki, D. Hirata, Y. Sugahara, K. Sumiyoshi, and I. Tanihata, Relativistic many body approach for unstable nuclei and supernova, *Nucl. Phys. A* **588**, c357 (1995).
- [70] N.-U. F. Bastian, D. Blaschke, T. Fischer, and G. Röpke, Towards a Unified Quark-Hadron Matter Equation of State for Applications in Astrophysics and Heavy-Ion Collisions, *Universe* **4**, 67 (2018), [arXiv:1804.10178 \[nucl-th\]](#).
- [71] M. Cierniak, T. Klähn, T. Fischer, and N.-U. Bastian, Vector-Interaction-Enhanced Bag Model, *Universe* **4**, 30 (2018), [arXiv:1802.03214 \[nucl-th\]](#).
- [72] T. Fischer, N.-U. F. Bastian, M.-R. Wu, P. Baklanov, E. Sorokina, S. Blinnikov, S. Typel, T. Klähn, and D. B. Blaschke, Quark deconfinement as a supernova explosion engine for massive blue supergiant stars, *Nature Astron.* **2**, 980 (2018), [arXiv:1712.08788 \[astro-ph.HE\]](#).
- [73] N.-U. F. Bastian, Phenomenological quark-hadron equations of state with first-order phase transitions for astrophysical applications, *Phys. Rev. D* **103**, 023001 (2021), [arXiv:2009.10846 \[nucl-th\]](#).
- [74] A. Bauswein, N.-U. F. Bastian, D. B. Blaschke, K. Chatziioannou, J. A. Clark, T. Fischer, and M. Oertel, Identifying a first-order phase transition in neutron star mergers through gravitational waves, *Phys. Rev. Lett.* **122**, 061102 (2019), [arXiv:1809.01116 \[astro-ph.HE\]](#).
- [75] M. A. R. Kaltenborn, N.-U. F. Bastian, and D. B. Blaschke, Quark-nuclear hybrid star equation of state with excluded volume effects, *Phys. Rev. D* **96**, 056024 (2017), [arXiv:1701.04400 \[astro-ph.HE\]](#).
- [76] D. Radice, A. Perego, S. Bernuzzi, and B. Zhang, Long-lived Remnants from Binary Neutron Star Mergers, *Mon. Not. Roy. Astron. Soc.* **481**, 3670 (2018), [arXiv:1803.10865 \[astro-ph.HE\]](#).
- [77] T. Dietrich, D. Radice, S. Bernuzzi, F. Zappa, A. Perego, B. Brügmann, S. V. Chaurasia, R. Dudi, W. Tichy, and M. Ujevic, CoRe database of binary neutron star merger waveforms, *Class. Quant. Grav.* **35**,



- 24LT01 (2018), [arXiv:1806.01625 \[gr-qc\]](#).
- [78] D. Radice, A. Perego, K. Hotokezaka, S. A. Fromm, S. Bernuzzi, and L. F. Roberts, Binary Neutron Star Mergers: Mass Ejection, Electromagnetic Counterparts and Nucleosynthesis, *Astrophys. J.* **869**, 130 (2018), [arXiv:1809.11161 \[astro-ph.HE\]](#).
  - [79] S. Bernuzzi, A. Nagar, T. Dietrich, and T. Damour, Modeling the Dynamics of Tidally Interacting Binary Neutron Stars up to the Merger, *Phys. Rev. Lett.* **114**, 161103 (2015), [arXiv:1412.4553 \[gr-qc\]](#).
  - [80] D. Radice, A. Perego, F. Zappa, and S. Bernuzzi, GW170817: Joint Constraint on the Neutron Star Equation of State from Multimessenger Observations, *Astrophys. J. Lett.* **852**, L29 (2018), [arXiv:1711.03647 \[astro-ph.HE\]](#).
  - [81] D. Radice, S. Bernuzzi, W. Del Pozzo, L. F. Roberts, and C. D. Ott, Probing Extreme-Density Matter with Gravitational Wave Observations of Binary Neutron Star Merger Remnants, *Astrophys. J. Lett.* **842**, L10 (2017), [arXiv:1612.06429 \[astro-ph.HE\]](#).
  - [82] A. Perego, S. Bernuzzi, and D. Radice, Thermodynamics conditions of matter in neutron star mergers, *Eur. Phys. J. A* **55**, 124 (2019), [arXiv:1903.07898 \[gr-qc\]](#).
  - [83] D. Radice and L. Rezzolla, THC: a new high-order finite-difference high-resolution shock-capturing code for special-relativistic hydrodynamics, *Astron. Astrophys.* **547**, A26 (2012), [arXiv:1206.6502 \[astro-ph.IM\]](#).
  - [84] D. Radice, L. Rezzolla, and F. Galeazzi, High-Order Fully General-Relativistic Hydrodynamics: new Approaches and Tests, *Class. Quant. Grav.* **31**, 075012 (2014), [arXiv:1312.5004 \[gr-qc\]](#).
  - [85] D. Radice, L. Rezzolla, and F. Galeazzi, Beyond second-order convergence in simulations of binary neutron stars in full general-relativity, *Mon. Not. Roy. Astron. Soc.* **437**, L46 (2014), [arXiv:1306.6052 \[gr-qc\]](#).
  - [86] A. S. Schneider, L. F. Roberts, and C. D. Ott, Open-source nuclear equation of state framework based on the liquid-drop model with Skyrme interaction, *Phys. Rev. C* **96**, 065802 (2017), [arXiv:1707.01527 \[astro-ph.HE\]](#).
  - [87] A. Bauswein, S. Blacker, V. Vijayan, N. Stergioulas, K. Chatziioannou, J. A. Clark, N.-U. F. Bastian, D. B. Blaschke, M. Cierniak, and T. Fischer, Equation of state constraints from the threshold binary mass for prompt collapse of neutron star mergers, *Phys. Rev. Lett.* **125**, 141103 (2020), [arXiv:2004.00846 \[astro-ph.HE\]](#).
  - [88] S. D. Tootle, L. J. Papenfort, E. R. Most, and L. Rezzolla, Quasi-universal Behavior of the Threshold Mass in Unequal-mass, Spinning Binary Neutron Star Mergers, *Astrophys. J. Lett.* **922**, L19 (2021), [arXiv:2109.00940 \[gr-qc\]](#).
  - [89] S. Köppel, L. Bovard, and L. Rezzolla, A General-relativistic Determination of the Threshold Mass to Prompt Collapse in Binary Neutron Star Mergers, *Astrophys. J. Lett.* **872**, L16 (2019), [arXiv:1901.09977 \[gr-qc\]](#).
  - [90] F. Zappa, S. Bernuzzi, D. Radice, A. Perego, and T. Dietrich, Gravitational-wave luminosity of binary neutron stars mergers, *Phys. Rev. Lett.* **120**, 111101 (2018), [arXiv:1712.04267 \[gr-qc\]](#).
  - [91] L. Lindblom, Spectral Representations of Neutron-Star Equations of State, *Phys. Rev. D* **82**, 103011 (2010), [arXiv:1009.0738 \[astro-ph.HE\]](#).
  - [92] M. F. Carney, L. E. Wade, and B. S. Irwin, Comparing two models for measuring the neutron star equation of state from gravitational-wave signals, *Phys. Rev. D* **98**, 063004 (2018), [arXiv:1805.11217 \[gr-qc\]](#).
  - [93] B. P. Abbott *et al.* (LIGO Scientific, Virgo), GW170817: Measurements of neutron star radii and equation of state, *Phys. Rev. Lett.* **121**, 161101 (2018), [arXiv:1805.11581 \[gr-qc\]](#).
  - [94] M. Hannam, P. Schmidt, A. Bohé, L. Haegel, S. Husa, F. Ohme, G. Pratten, and M. Pürrer, Simple Model of Complete Precessing Black-Hole-Binary Gravitational Waveforms, *Phys. Rev. Lett.* **113**, 151101 (2014), [arXiv:1308.3271 \[gr-qc\]](#).
  - [95] T. Dietrich, S. Bernuzzi, and W. Tichy, Closed-form tidal approximants for binary neutron star gravitational waveforms constructed from high-resolution numerical relativity simulations, *Phys. Rev. D* **96**, 121501 (2017), [arXiv:1706.02969 \[gr-qc\]](#).
  - [96] T. Dietrich *et al.*, Matter imprints in waveform models for neutron star binaries: Tidal and self-spin effects, *Phys. Rev. D* **99**, 024029 (2019), [arXiv:1804.02235 \[gr-qc\]](#).
  - [97] E. Poisson, Gravitational waves from inspiraling compact binaries: The quadrupole-moment term, *Phys. Rev. D* **57**, 5287 (1998).
  - [98] K. G. Arun, A. Buonanno, G. Faye, and E. Ochsner, Higher-order spin effects in the amplitude and phase of gravitational waveforms emitted by inspiraling compact binaries: Ready-to-use gravitational waveforms, *Phys. Rev. D* **79**, 104023 (2009), [Erratum: *Phys. Rev. D* **84**, 049901 (2011)], [arXiv:0810.5336 \[gr-qc\]](#).
  - [99] B. Mikoczi, M. Vasuth, and L. A. Gergely, Self-interaction spin effects in inspiraling compact binaries, *Phys. Rev. D* **71**, 124043 (2005), [arXiv:astro-ph/0504538](#).
  - [100] A. Bohé, G. Faye, S. Marsat, and E. K. Porter, Quadratic-in-spin effects in the orbital dynamics and gravitational-wave energy flux of compact binaries at the 3PN order, *Class. Quant. Grav.* **32**, 195010 (2015), [arXiv:1501.01529 \[gr-qc\]](#).
  - [101] C. K. Mishra, A. Kela, K. G. Arun, and G. Faye, Ready-to-use post-Newtonian gravitational waveforms for binary black holes with nonprecessing spins: An update, *Phys. Rev. D* **93**, 084054 (2016), [arXiv:1601.05588 \[gr-qc\]](#).
  - [102] A. Bohé *et al.*, Improved effective-one-body model of spinning, nonprecessing binary black holes for the era of gravitational-wave astrophysics with advanced detectors, *Phys. Rev. D* **95**, 044028 (2017), [arXiv:1611.03703 \[gr-qc\]](#).
  - [103] S. Husa, S. Khan, M. Hannam, M. Pürrer, F. Ohme, X. Jiménez Forteza, and A. Bohé, Frequency-domain gravitational waves from nonprecessing black-hole binaries. I. New numerical waveforms and anatomy of the signal, *Phys. Rev. D* **93**, 044006 (2016), [arXiv:1508.07250 \[gr-qc\]](#).
  - [104] A. Nagar *et al.*, Time-domain effective-one-body gravitational waveforms for coalescing compact binaries with nonprecessing spins, tides and self-spin effects, *Phys. Rev. D* **98**, 104052 (2018), [arXiv:1806.01772 \[gr-qc\]](#).
  - [105] S. Akcay, S. Bernuzzi, F. Messina, A. Nagar, N. Ortiz, and P. Rettengo, Effective-one-body multipolar waveform for tidally interacting binary neutron stars up to merger, *Phys. Rev. D* **99**, 044051 (2019), [arXiv:1812.02744 \[gr-qc\]](#).
  - [106] S. van der Walt, S. C. Colbert, and G. Varoquaux,



- The NumPy Array: A Structure for Efficient Numerical Computation, *Comput. Sci. Eng.* **13**, 22 (2011), [arXiv:1102.1523 \[cs.MS\]](#).
- [107] P. Virtanen *et al.*, SciPy 1.0: Fundamental Algorithms for Scientific Computing in Python, *Nature Methods* **17**, 261 (2020).
- [108] J. D. Hunter, Matplotlib: A 2d graphics environment, *Computing in Science & Engineering* **9**, 90 (2007).
- [109] M. L. Waskom, seaborn: statistical data visualization, *Journal of Open Source Software* **6**, 3021 (2021).
- [110] K. Wette, SWIGLAL: Python and Octave interfaces to the LALSuite gravitational-wave data analysis libraries, *SoftwareX* **12**, 100634 (2020).
- [111] LIGO Scientific Collaboration, Virgo Collaboration, and KAGRA Collaboration, *LVK Algorithm Library - LALSuite*, Free software (GPL) (2018).